International Journal of
Optics and Photonics (IJOP)

A pubication of Optics and Photonics Society of Iran (OPSI)

WINTER-SPRING 2016 VOLUME 10 NUMBER 1

Papers' Titles and Authors **Pages**

Design and Construction of a Seismometer Based on the Moiré Technique: Detailed Theoretical Analysis, Experimental Apparatus, and Primary Results *3-10*

Saifollah Rasouli, Shamsedin Esmaeili, and Farhad Sobouti

Simulation of Light-Nanowire Interaction in the TE Mode Using Surface Integral Equations *11-18*

Masoud Rezvani Jalal and Maryam Fathi Sepahvand

All-Optical Reconfigurable-Tunable 1×N Power Splitter Using Soliton Breakup *19-29*

Amin Ghadi and Saeed Mirzanejhad

Tunable Schottky Barrier in Photovoltaic BiFeO3 Based Ferroelectric Composite Thin Films *31-35*

Seyed Mohammad Hosein Khalkhali, Mohammad Mehdi Tehranchi, and Seyedeh Mehri Hamidi

Self-Fields Effects on Gain in a Helical Wiggler Free Electron Laser with Ion-Channel Guiding and Axial Magnetic Field *37-46*

Hasan Ehsani Amri and Taghi Mohsenpour

Use of Zernike Polynomials and SPGD Algorithm for Measuring the Reflected Wavefronts from the Lens Surfaces *47-53*

Roghayeh Yazdani, Sebastian Petsch, Hamid Reza Fallah, and Morteza Hajimahmoodzade

A Systematic Approach to Photonic Crystal Based Metamaterial Design *55-64*

Saeed Pahlavan and Vahid Ahmadi

In the name of God, the Compassionate, the Merciful

International Journal of Optics and Photonics (IJOP)

ISSN: 1735-8590

International Journal of Optics and Photonics (IJOP) is an open access journal published by the Optics and Photonics Society of Iran (OPSI). It is published online semiannually and its language is English. All publication expenses are paid by OPSI, hence the publication of paper in IJOP is **free of charge.**

For information on joining the OPSI and submitting papers, please visit **http://www.ijop.ir, http://www.opsi.ir**, or contact the society secretarial office via **info@opsi.ir**.

All correspondence and communication for Journal should be directed to:

IJOP Editorial Office
Optics and Photonics Society of Iran (OPSI)
P O Box 14395-115
Tehran, 1439663741, Iran
Phone: (+98) 21-44255936
Fax: (+98) 21-44255937
Email: info@ijop.ir

All-Optical Reconfigurable-Tunable 1×N Power Splitter Using Soliton Breakup

Amin Ghadi* and Saeed Mirzanejhad

Department of Physics, University of Mazandaran, Babolsar, Iran

***Corresponding Author Email:** a.ghadi@umz.ac.ir

Received: Apr. 4, 2015, Revised: June 21, 2015, Accepted: Aug. 8, 2015, Available online: Apr. 30, 2016.

ABSTRACT— In this paper, we numerically simulated a glass-based all-optical 1×N power splitter with eleven different configurations using soliton breakup in a nonlinear medium. It is shown that in addition to reconfigurability of the proposed splitter, its power splitting ratio is tunable up to some extent values too. Nonlinear semivectorial iterative finite difference beam propagation method (IFD-BPM) with inclusion of two photon absorption (TPA) effects is applied to simulate the soliton propagation at different mode power. It is shown that operation of the proposed splitter depends on input mode power and an all-optical reconfigurable-tunable functional device is designed with nonlinear optical (NLO) property of a simple structure.

KEYWORDS: Nonlinear optics, integrated optics; Optical switching devices; Spatial solitons; Ultrafast nonlinear optics.

I. INTRODUCTION

One of the very interesting features of controlling light by light is all-optical integrated photonic devices which are key elements in ultrafast data processing. One of the usual key to reach this demand is using solitons in an intensity dependent medium in which diffraction and self-focusing balances each other [1, 2]. Many all-optical photonic switches based on spatial soliton interactions such as all-optical switch based on the spatial soliton repulsion [3], all-optical 1 × N switching [4], wavelength auto-router [5], soliton switching in a Kerr coupler [6], polarization beam splitter [7], switching of discrete solitons in waveguide arrays [8], soliton switching in a fiber [9], nonlinear directional coupler [10] and logic gates [11] are proposed. In addition to diffractionless propagation, many diffractive switching devices and power splitters based on multimode interference coupler [12-16] are proposed. As regards Kerr effect and TPA have efficient effects on soliton propagation [17-21], we intended to base our model on spatial soliton propagation in an intensity dependent medium with TPA effects. With regard to many investigations, study of stable behavior of solitons such as self-trapping and diffraction was devoted to planar waveguides [21-23], we deal with our model in two-dimensional (2D) case. Although, nonlinear Schrodinger equation is commonly used to study soliton propagation [9, 10, 21, 23], solving Maxwell's equations in nonlinear medium by beam propagation method [24] or finite difference time domain [25] are accurate and powerful methods to simulate solitons in real optical medium. Therefore, we extended the same approach used in iterative finite element beam propagation method (IFE-BPM) [26] with inclusion of TPA to study spatial solitons, but we apply it with finite difference scheme in our simulations.

In this paper we first develop IFE-BPM to IFD-BPM with inclusion of nonlinear loss induced by TPA to simulate spatial solitons in an intensity dependent medium. Then we compare our IFD-BPM with solving a problem that is previously solved by wide-angle IFE-

BPM. Next, we describe the structure of our all-optical glass-based power splitter, and design eleven different configurations by soliton breakup in a simple structure. The splitting power ratios depend on input mode power. We show that not only our splitter is reconfigurable but also it is tunable to some extent values. Unlike to similar proposed splitters [3-5], we include TPA in our investigation, too. Finally, the paper is concluded.

II. BASIC EQUATIONS

For simplicity, we restrict our formulation to the 2D case and TE-polarization. Therefore we consider planar (2D) nonlinear optical waveguides, where x and z are the transverse and the propagation directions, respectively, and there is no variation in the y direction ($\partial/\partial y \equiv 0$). Under these assumptions we obtain the following basic wave equation for y-directed electric field E_y of TE mode as

$$\frac{\partial^2 E_y}{\partial z^2} + \frac{\partial^2 E_y}{\partial x^2} + n^2 k_0^2 E_y = 0, \quad (1)$$

where k_0 is the wavenumber in vacuum and n is the intensity dependent refractive index of medium given by [26]

$$n = n_0 + \frac{1}{2} c \varepsilon_0 n_0 n_{nl} |E|^2. \quad (2)$$

Here, c is the light velocity, ε_0 is the permittivity of free space, n_0 is the linear refractive index, n_{nl} is the nonlinear refractive index Kerr coefficient [27], and E is the electric field vector. With using slowly varying approximation, we divide the principal field $E_y(x,z)$ propagating in z direction into the slowly varying envelope function $\phi(x,z)$ and very fast oscillatory phase term $exp(-i\beta z)$ as

$$E_y(x,z) = \phi(x,z) e^{i\beta z}, \quad (3)$$

where $\beta = n_{eff} k_0$ that n_{eff} is the effective index. With substitute the electric field into Eq. (1) and taking Fresnel approximation [28] we obtain the following beam propagation equation for the slowly varying complex amplitude $\phi(x,z) \equiv \phi$.

$$2i\beta \frac{\partial \varphi}{\partial z} = \frac{\partial^2 \varphi}{\partial x^2} + k_0^2 \left(n^2 - n_{eff}^2 \right) \varphi. \quad (4)$$

With equidistant discretization of x coordinate by $x = p\Delta x$ and z coordinate by $z = l\Delta z$ that l and p are integers and Δx and Δz are the step size long x and z directions respectively, we represent the field distribution at each point with $\phi(p\Delta x, l\Delta z) \equiv \phi_p^l$. Finally, the semivectorial finite difference beam propagation method of Eq. (4) with using Crank-Nicholson scheme [28-30] yields

$$-\phi_{p-1}^{l+1} + A_+ \phi_p^{l+1} - \phi_{p+1}^{l+1} = \phi_{p-1}^{l} + A_- \phi_p^{l} + \phi_{p+1}^{l}, \quad (5)$$

where the coefficient $A_\pm$ in each step of propagation is given by

$$A_\pm = \pm 2 + \frac{4i\beta\Delta x^2}{\Delta z} \mp k_0^2 \Delta x^2 \left(n^2 - n_{eff}^2 \right). \quad (6)$$

With solving Eq. (5), we will achieve electric filed distribution of each step by its value in previous step. To include intensity dependent loss induced by TPA we consider an intensity dependent absorption coefficient [27] in each step by

$$\alpha = \alpha_0 + \frac{1}{2} c \varepsilon_0 n_0 \alpha_{nl} |E|^2. \quad (7)$$

Here α_0 is linear absorption coefficient of medium and α_{nl} is nonlinear absorption coefficient [27] owing to TPA. We include the intensity dependent loss in each step with multiplying the attenuation factor $exp(-\alpha\Delta z)$ on the achieved electric field distribution from Eq. (5) by

$$\tilde{\phi}_p^{l+1} = e^{-\alpha\Delta z}\phi_p^{l+1}, \tag{8}$$

where $\tilde{\phi}_p^{l+1}$ represents the new field distribution achieved from its previous value ϕ_p^{l+1} in each step. To deal with the intensity dependent refractive index and absorption coefficient, an additional calculation step must be added to the iterative scheme as defined in [26]. The nonlinear refractive index and absorption coefficient in each point at the (l+1)th step is modified as from the field patterns at the l-th and (l+1)th steps.

$$n = n_0 + \frac{1}{2}c\varepsilon_0 n_0 n_{nl}\left|\frac{\tilde{\phi}_p^{l+1} + \tilde{\phi}_p^{l}}{2}\right|^2. \tag{9}$$

$$\alpha = \alpha_0 + \frac{1}{2}c\varepsilon_0 n_0 \alpha_{nl}\left|\frac{\tilde{\phi}_p^{l+1} + \tilde{\phi}_p^{l}}{2}\right|^2. \tag{10}$$

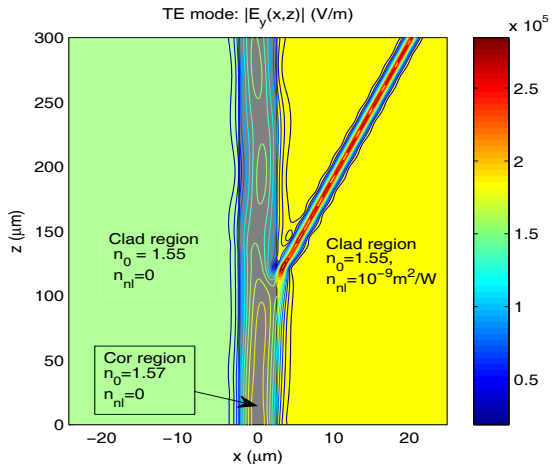

Fig. 1: Two Dimensional nonlinear semivectorial IFD-BPM in lossless three layered media. The dark region in the center shows linear core with 5μm width, the green region in the left hand side is linear clad with 22.5 μm width and the yellow region in the right side is lossless nonlinear clad with 22.5 μm width. Propagation of a fundamental mode with power $P_0 = 300W/m$ and effective index $n_{eff} = 1.5670$ at $\lambda = 1.3\mu m$ excite a soliton in the nonlinear clad. The simulation is in good agreement with the same simulation by wide-angle nonlinear IFE-BPM in Fig. (6-a) of [26].

The solution for the (l+1)th step is recalculated with the modified nonlinear refractive index Eq. (9) and absorption coefficient Eq. (10). This scheme is continued until the solution at the (l+1)th step converges. It is necessary an iterative procedure included to ensure the local permittivity and absorption are converge with the local electric field. In this case, Eq. (5) should be solved iteratively until the following convergence condition is satisfied.

$$Max\left[\frac{\tilde{\phi}_p^{*l+1} - \tilde{\phi}_p^{l+1}}{\tilde{\phi}_p^{*l+1}}\right] < \delta_{tol}, \tag{11}$$

where δ_{tol} is the required tolerance for convergence and $\tilde{\phi}_p^{*l+1}$ is the updated value of field distribution achieved in each step. In order to suppress unwanted reflections from the edges, we implement a transparent boundary condition (TBC) at the edges of the computational domain [31].

III. Comparison with Wide-Angle Nonlinear IFE-BPM

Our derived nonlinear semivectorial IFD-BPM relations in previous section are based on Fresnel approximation. In this section we consider a solved problem with wide-angle nonlinear IFE-BPM in [26] and compare it with our achieved simulation by nonlinear IFD-BPM.

Figure (1) shows contour plot of 2D beam propagation in three layered lossless waveguide ($\alpha \equiv 0$). The dark region placed in the center is linear core waveguide with linear refractive index $n_0 = 1.57$ and 5 μm width. The yellow region in the right hand side is nonlinear clad with linear refractive index $n_0 = 1.55$, nonlinear refractive index $n_{nl} = 10^{-9} m^2/W$ [26] and 22.5 μm width. The green region in the left hand side is linear clad with linear refractive index $n_0 = 1.55$ and 22.5 μm width. In this example the absorption coefficient is considered $\alpha = 0$ for all regions.

The incident wave in the core (dark region) is the fundamental mode with $P_0 = 300W/m$ power at wavelength $\lambda = 1.3\mu m$ with effective index $n_{eff} = 1.5670$. Discretization of simulation along x and z directions are $\Delta x = 62.5nm$ and $\Delta z = 1\mu m$ respectively. The convergence criterion used in this simulation is $\delta_{tol} = 10^{-5}$ and for the edges of the computational window TBC [31] is used too. Our nonlinear semivectorial IFD-BPM simulation shows that the incident wave in the core excite a soliton in the nonlinear clad and it diverges from the core with propagation along z. The propagation of the beam resulted by our simulation is in good agreement with the same simulation achieved by wide-angle nonlinear semivectorial IFE-BPM in Fig (6-a) of [26].

IV. Power Splitter Structure

Formation of solitons require high light powers in medium with low loss effects. Optical glasses and semiconductors with intensity dependent optical characteristics are usually used to soliton propagation. Both materials have a specific advantage and disadvantage with respect to another. Nonlinear absorption coefficient of glass $\alpha_{nl} = 2.3\times10^{-14} m/W$ [23] is lower than semiconductors [27] and this may be an advantage of glasses with respect to semiconductors. On the other hand, Kerr coefficient of the glass $n_{nl} = 3.4\times10^{-20} m^2/W$ [23] is lower than semiconductors and this may be a disadvantage of glasses with respect to semiconductors. Because the required light power to form a spatial soliton in glasses will be more than semiconductors. Anyway, in this section we considered a symmetric glass-based power splitter that is schematically depicted in Fig. (2). It should be notified that this figure is stretched vertically for better view and the real size of the problem can be found from the vertical and horizontal axes. The splitter mainly contains two parts. The first part is considered with an input lossless linear waveguide that is shown with red color in Fig. (2) with 9 μm width, 5 μm length and linear refractive index $n_0 = 1.537$. This input injects the fundamental mode of waveguide to the nonlinear region. The second part with yellow color in Fig. (2) is nonlinear medium which is composed of propagation and output regions. The propagation region has 200 μm length and 40 μm width and the output region with 134 μm length is composed of nine output waveguides. We assumed that the yellow colored region is glass-based medium with linear refractive index $n_0 = 1.537$, nonlinear refractive index $n_{nl} = 3.4\times10^{-20} m^2/W$, linear absorption $\alpha_0 = 10m^{-1}$ and nonlinear absorption $\alpha_{nl} = 2.3\times10^{-14} m/W$ [23]. The clad region with green color is assumed made of a lossless linear medium with linear refractive index $n_0 = 1.53$. The whole splitter structure is geometrically symmetric with respect to $x = 0$ axis.

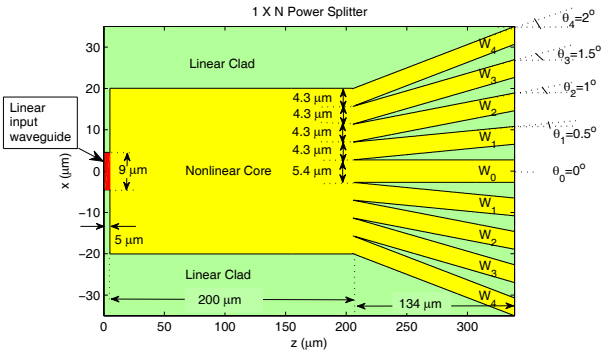

Fig. 2: Schematic of a symmetric 1×N power splitter with nonlinear core and linear clad. The red colored region shows input linear waveguide with 9 μm width, 5 μm length and linear refractive index $n_0 = 1.537$ which injects the fundamental mode of waveguide to nonlinear region. The yellow colored region is nonlinear core with linear refractive index $n_0 = 1.537$, nonlinear refractive index $n_{nl} = 3.4\times10^{-20} m^2/W$, linear absorption $\alpha_0 = 10m^{-1}$ and nonlinear absorption $\alpha_{nl} = 2.3\times10^{-14} m/W$. Output of splitter is composed of nine output waveguides which are determined with $W_{0\text{-}4}$. The central output waveguide W_0 with 5.4 μm width is considered horizontally and the other output waveguides are identical and mutually symmetric that are shown with W_1, W_2, W_3 and W_4 and slop angles θ_1=0.5°,

θ_2=1°, θ_3=1.5° and θ_4=2° respectively. The green colored region shows lossless linear clad with linear refractive index $n_0 = 1.53$.

The central output waveguide W_0 with 5.4 μm width is considered horizontally that is shown in Fig. (2) with slop angle θ_0=0°. The other eight output waveguides are identical and mutually symmetric that are shown in Fig. (2) with W_1, W_2, W_3 and W_4 and slop angles θ_1=0.5°, θ_2=1°, θ_3=1.5° and θ_4=2° respectively. The input port of the splitter launches the fundamental mode of waveguide to the nonlinear region with wavelength $\lambda = 0.62\mu m$, effective index $n_{eff} = 1.5367$ and power P_0. Discretization along x and z directions are $\Delta x = 62.5nm$ and $\Delta z = 0.31\mu m$ respectively, the convergence criterion is $\delta_{tol} = 10^{-5}$ and for the edges of the computational window TBC [31] is used too. With setting the power of incident mode we can breakup a spatial soliton and design a tunable splitter which its operation depends on input mode power. We define coupling efficiency κ_i as a ratio of the power of each output waveguides p_i over the input mode power P_0 as:

$$\kappa_i = \frac{p_i}{P_0}, \quad i = 0,1,2,3,4. \tag{12}$$

To determine "on" and "off" states for the output waveguides, we define a threshold coupling efficiency with value $\kappa_t = 0.01$. In this way, when the value of coupling efficiency of each output waveguides be above threshold $\kappa_i \geq \kappa_t$ we regard the output waveguide is "on" and when be below threshold $\kappa_i < \kappa_t$ we regard the output waveguide is "off".

A. *1×1 splitter*

Figure (3) shows nonlinear semivectorial IFD-BPM simulation of the input fundamental mode with $P_0 = 270GW/m$. With this input mode power nonlinear self-focusing sets in, and the spatial width of the mode begins to narrow in space as it propagates until the mode profile at the center output waveguide W_0 collapses to smaller dimensions than the input mode. In this way, the mode propagates in a fundamental soliton fashion which diffraction and self-focusing can balance each other and the mode becomes self-trapped through the splitter. Also, it seems that the walls of the output waveguide W_1 may has an effect on decreasing width of the input mode profile. Anyway, this input mode power is suitable for our purpose. The main fragment of the input power transmits from the center output waveguide with $\kappa_0 = 0.4621$. Coupling efficiency of the other output waveguides are lower than threshold κ_t that are shown in the right hand side of Fig. (3). Hence, this configuration designs 1×1 splitter. We have the same configuration with different coupling efficiencies for the range of input mode power about $257GW/m \leq P_0 \leq 285GW/m$. Tunablility of the coupling efficiency of the output W_0 in this interval is about $0.5061 \leq \kappa_0 \leq 0.4751$.

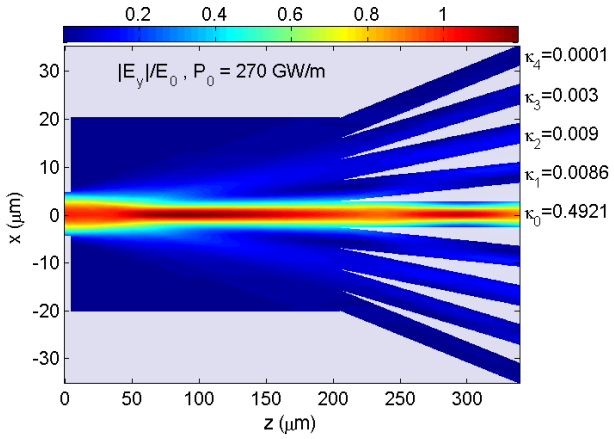

Fig. 3: Magnetization Nonlinear semivectorial IFD-BPM simulation of 1×1 splitter. The core and clad regions are shown with dark-blue and bright-blue colors respectively. The input fundamental mode with power $P_0 = 270GW/m$ propagates like a first fundamental soliton. The main fragment of the input mode power transmits from the central output waveguide W_0 and the other outputs are regarded "off".

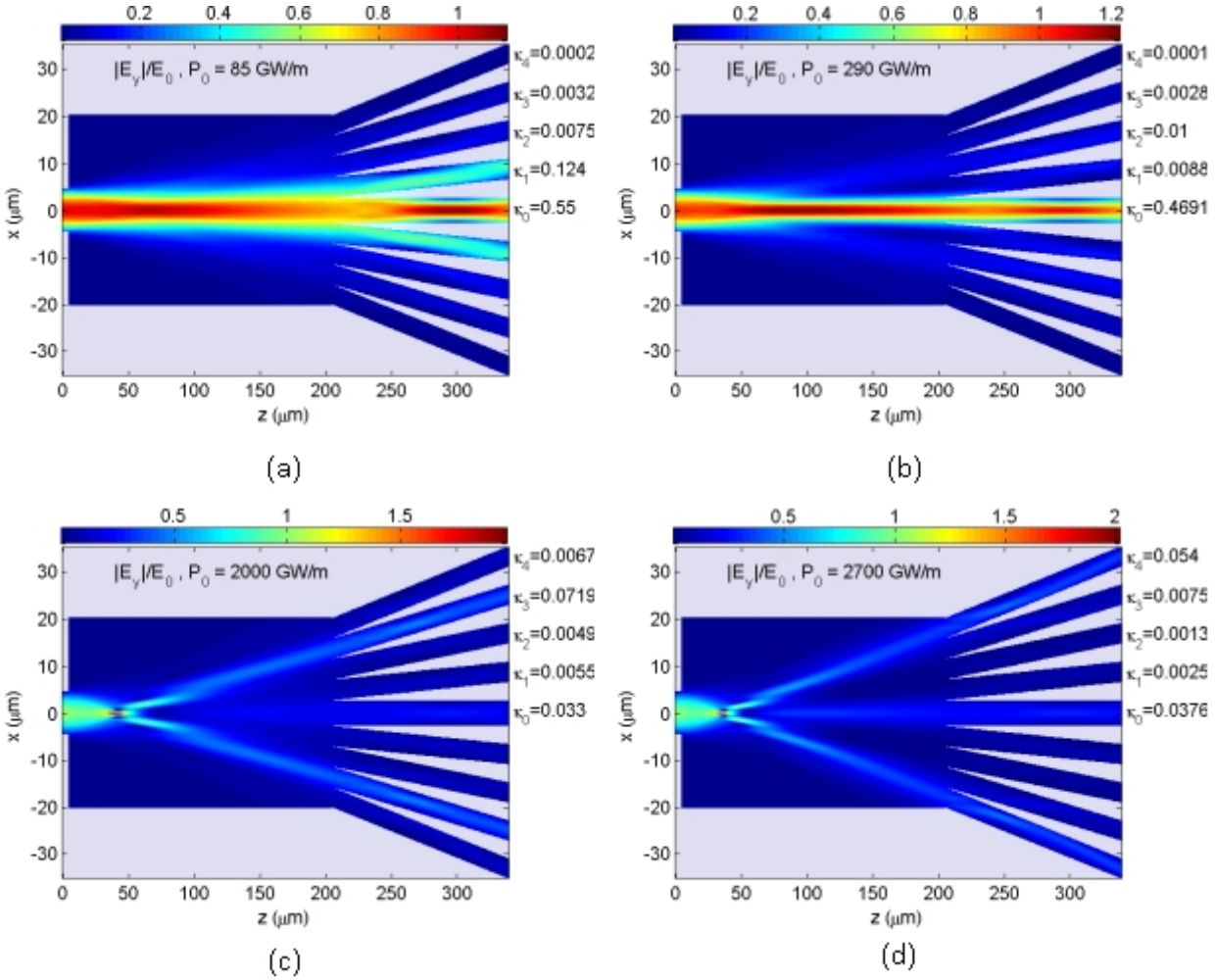

Fig. 4: Nonlinear semivectorial IFD-BPM simulation of 1×3 splitter with four configurations. (a) Input mode power $P_0 = 85GW/m$ turns "on" the outputs W_0 and W_1 with coupling efficiency above threshold. (b) Input mode power $P_0 = 290GW/m$ turns "on" the outputs W_0 and W_2 with coupling efficiency above threshold. (c) An intense input mode power $P_0 = 2000GW/m$ turns "on" the outputs W_0 and W_3 with coupling efficiency above threshold. (d) An intense input mode power $P_0 = 2700GW/m$ turns "on" the outputs W_0 and W_4 with coupling efficiency above threshold.

B. *1×3 splitter*

Figure (4) shows four different configurations of 1×3 splitter which is achieved by different input mode power. The first configuration is achieved with input mode power $P_0 = 85GW/m$ that is shown in Fig. (4-a). At this input mode power TPA effects is weak and diffraction dominates partially over self-focusing so that the interplay among those lead to route the main power of the input mode to three output waveguides. The greatest fragment of the mode power transmits from the center output waveguide W_0 with coupling efficiency $\kappa_0 = 0.55$ and the smaller fragment transmits from the output W_1 with coupling efficiency $\kappa_1 = 0.124$ that both are above threshold. Coupling efficiency of the other outputs are below threshold that is shown in the right hand side of Fig. (4-a) and hence those are regarded "off".

The second configuration is achieved with increasing the input mode power to $P_0 = 290GW/m$ as shown in Fig. (4-b). At this input the main portion of the mode power in the center profile propagates like a fundamental soliton. Additionally, a small fragment of the mode power begins to broaden owing to the high-intensity center of the mode

experiences more intensity-dependent loss than the lower-intensity wings. Therefore, the small power wings of the spatial profile split off and diverge from the central soliton channel. This phenomenon leads to rout the main power of the mode into the center output W_0 with $\kappa_0 = 0.4691$ and the two very smaller fragments into the W_2 outputs with $\kappa_2 = 0.01$. Coupling efficiency of the other outputs are below threshold and hence those are regarded "off".

With increasing the input mode power to $P_0 = 2000GW/m$ the third configuration can be achieved with intense NLO effects as shown in Fig. (4-c). As the mode power increases, it enhances NLO effects and leads to break up the soliton into two or more fundamental solitons that separate at a rate that depends on the soliton power and strength of NLO effects. In this case, the two diverging peaks have more power than the central peak and turn "on" symmetrically the two outputs W_3 with coupling efficiency $\kappa_3 = 0.0719$. The central peak turns "on" the central output W_0 with coupling efficiency $\kappa_0 = 0.033$.

To turn "on" the output W_4 we have to increase the input mode power to $P_0 = 2700GW/m$ as shown in Fig. (4-d). Similar to previous, the strong loss induced by enhanced TPA with strong Kerr effect in the center profile of the mode breaks the soliton into three fragments which are more diverging than Fig. (4-c). Coupling efficiency of the center output W_0 decreases to $\kappa_0 = 0.0376$ and the two W_4 outputs increases to $\kappa_4 = 0.054$ which are above threshold. Coupling efficiency of the other outputs are below threshold. Therefore with setting the input mode power four configurations are achieved for 1×3 splitter with one simple structure.

C. *1×4 splitter*

Figure (5) shows a configuration for 1×4 splitter which is achieved by input mode power $P_0 = 1100GW/m$. The profile of the input mode breaks into a two-peaked symmetric fragments which is resulted by strong NLO effects in the center profile of the mode. In this configuration coupling efficiency of the four output waveguides, W_1 and W_2, are above threshold with $\kappa_1 = 0.0732$ and $\kappa_2 = 0.0643$ respectively and the others are below threshold. We could find only one configuration for 1×4 splitter. We will have the same configuration with different coupling efficiencies for the range of input mode power about $938GW/m \le P_0 \le 1130GW/m$. Tunability of the coupling efficiency of the four output waveguides, W_1 and W_2, in this interval are respectively about $0.0655 \le \kappa_1 \le 0.1134$ and $0.0691 \le \kappa_2 \le 0.0378$.

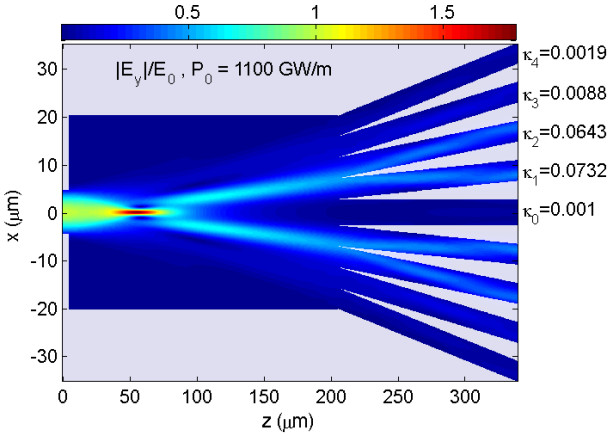

Fig. 5: Nonlinear semivectorial IFD-BPM simulation of 1×4 splitter. Input mode power $P_0 = 1100GW/m$ case to set in self-focusing and then breakup into two equal diverging peak fragments. This soliton breakup turns "on" the outputs W_1 and W_2 with coupling efficiency above threshold.

D. *1×5 splitter*

Three configurations are found for 1×5 splitter that are shown in Fig. (6). Figure (6-a) shows the input mode power $P_0 = 600GW/m$ that its profile initially collapses to smaller dimensions than the input owing to self-focusing and then disperses widely due to contribution of TPA and diffraction effects. Coupling efficiencies of the output

waveguides W_0, W_1 and W_2 are respectively $\kappa_0 = 0.1517$, $\kappa_1 = 0.1074$ and $\kappa_2 = 0.0227$.

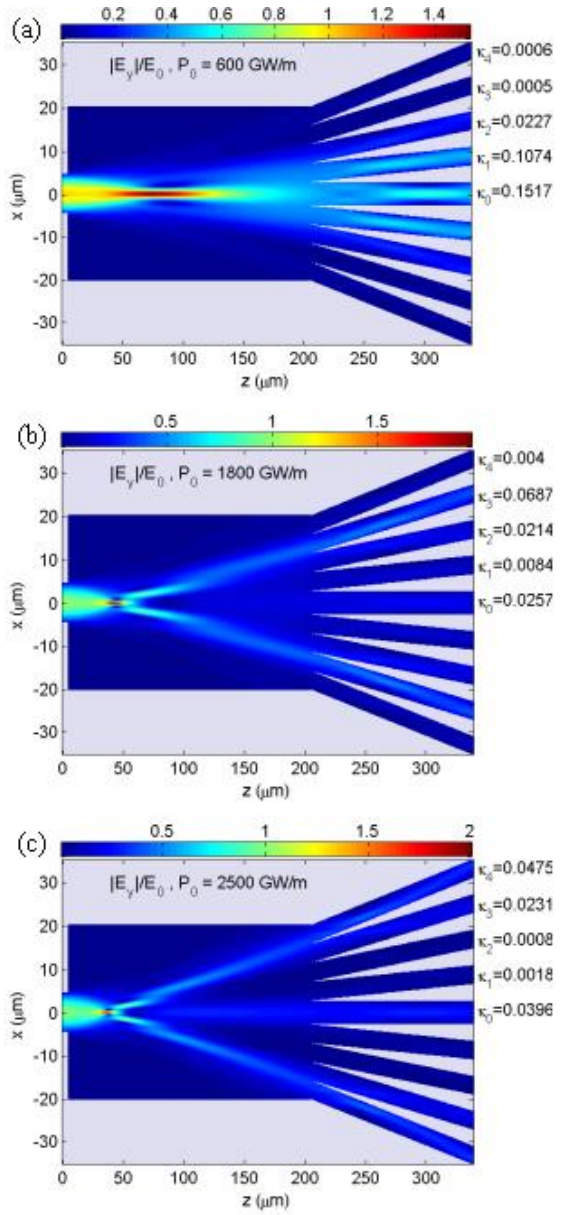

Fig. 6: Nonlinear semivectorial IFD-BPM simulation of 1×5 splitter with three configurations. (a) Input mode power $P_0 = 600GW/m$ become self-focused and then greatly dispersed owing to TPA effects which leads to turns "on" the outputs W_0, W_1 and W_2 with coupling efficiency above threshold. (b) An intense input mode power $P_0 = 1800GW/m$ become self-focused and then breaks into three symmetric peak fragments which turns "on" the outputs W_0, W_2 and W_3 with coupling efficiency above threshold. (c) With increase of the input mode power to $P_0 = 2500GW/m$ divergence of the peaks becomes more and turns "on" the outputs W_0, W_3 and W_4 with coupling efficiency above threshold.

The other coupling efficiencies are lower than threshold and hence W_3 and W_4 are regarded "off". The second configuration is achieved with increasing the input mode power to $P_0 = 1800GW/m$ as shown in Fig. (6-b). As can be seen, the two symmetric diverging peak fragments turns "on" the outputs W_0, W_2 and W_3 with coupling efficiency about $\kappa_0 = 0.0257$, $\kappa_2 = 0.0214$ and $\kappa_3 = 0.0687$.

The other coupling efficiencies are below threshold and so those are regarded "off". The third configuration is achieved with increasing the input mode power to $P_0 = 2500GW/m$ as shown in Fig. (6-c). Similar to the same scenario in Fig. (4-d), the strong NLO effects in the center profile of the mode breaks the soliton into three fragments which routes the separated peaks to the outputs W_0, W_3 and W_4 with coupling efficiencies $\kappa_0 = 0.0396$, $\kappa_3 = 0.0231$ and $\kappa_4 = 0.0475$ respectively. Coupling efficiency of the outputs W_1 and W_2 are lower than threshold and hence those are regarded "off".

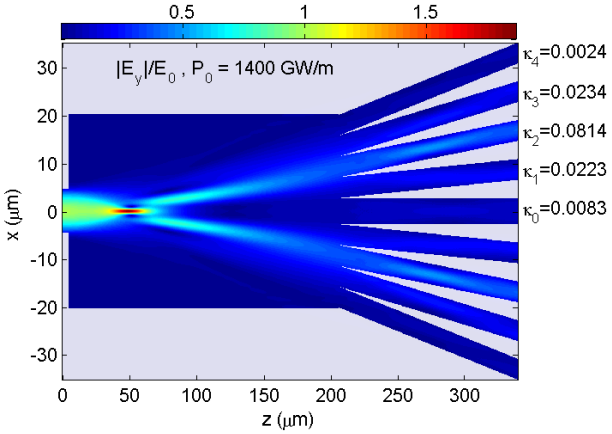

Fig. 7: Nonlinear semivectorial IFD-BPM simulation of 1×6 splitter with input mode power $P_0 = 1400GW/m$. After a self-focusing the mode profile breaks into two equal diverging peaks which leads to turns "on" the outputs W_1, W_2 and W_3 with coupling efficiency above threshold.

E. *1×6 splitter*

Only one configuration is found for 1×6 splitter with mode power $P_0 = 1400GW/m$ as shown in Fig. (7). The mode profile after an

intense self-focusing breaks into two-peaked fragments due to NLO effects and then turns "on" the outputs W_1, W_2 and W_3 with coupling efficiencies $\kappa_1 = 0.0223$, $\kappa_2 = 0.0814$ and $\kappa_3 = 0.0234$ respectively. Coupling efficiencies of the other outputs are lower than threshold and hence those are regarded "off". For the range input mode power about $1135GW/m \le P_0 \le 1437GW/m$ we have the same configuration but with different coupling efficiencies. Tunability of the coupling efficiencies of the outputs W_1, W_2 and W_3 in this interval are respectively about $0.0642 \le \kappa_1 \le 0.0198$, $0.0699 \le \kappa_2 \le 0.0790$ and $0.0101 \le \kappa_3 \le 0.0263$.

F. *1×7 splitter*

Similar to previous, only one configuration is achieved for 1×7 splitter with increasing the input mode power to $P_0 = 1500GW/m$ as shown in Fig. (8).

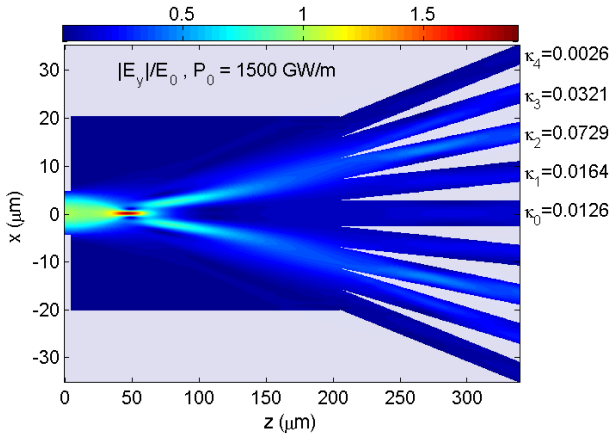

Fig. 8: Nonlinear semivectorial IFD-BPM simulation of 1×7 splitter with input mode power $P_0 = 1500GW/m$. After a self-focusing the mode profile breaks into two equal diverging peaks which leads to turns "on" the outputs W_0, W_1, W_2 and W_3 with coupling efficiency above threshold.

As the power is increased, the enhanced NLO effects in the center profile of the mode and causes to diverge the two separated peaks more efficient than in Fig. (7). Coupling efficiencies of the outputs W_0, W_1, W_2 and W_3 are respectively equal to $\kappa_0 = 0.0126$, $\kappa_1 = 0.0164$, $\kappa_2 = 0.0729$ and $\kappa_3 = 0.0321$. Coupling efficiency of the output W_4 is lower than threshold and hence it is regarded "off". For the range of mode power about $1439GW/m \le P_0 \le 1720GW/m$ we have the same configuration but with different coupling efficiency. Tunability of the coupling efficiencies of the outputs W_0, W_1, W_2 and W_3 in this interval are respectively about $0.0100 \le \kappa_0 \le 0.0224$, $0.0197 \le \kappa_1 \le 0.0100$, $0.0789 \le \kappa_2 \le 0.0351$, and $0.0264 \le \kappa_3 \le 0.0610$.

V. CONCLUSION

In this investigation, at first we extended nonlinear semivectorial IFD-BPM with inclusion of TPA effect. Secondly, we proposed a glass-based symmetric power splitter with nonlinear core. We numerically showed that reconfigurable 1×N power splitter can be designed by a simple structure via soliton breakup. Unlike to similar previous models, we took into consideration loss effects induced by TPA in soliton propagation. It is numerically shown that the enhanced NLO effects enable us to breaks the soliton desirably into some peaks which its fragments and divergence depends on input mode power. In our model, this property enabled us to design the all-optical 1×N power splitter. Eleven different configurations are achieved by a simple symmetric structure in which the power ratios are tunable to some extent values. This model can be potential key component to generate the ultrafast all-optical functional devices such as switches, routers and tunable power splitters which its operation depends on its input mode power.

REFERENCES

[1] G.I.A. Stegeman, D.N. Christodoulides, and M. Segev, "Optical spatial solitons: historical perspectives," IEEE J. Selec. Top. in Quantum Electron. Vol. 6, No. 6, pp. 1419-1427, 2000.

[2] Y.S. Kivshar and G.P. Agrawal, *Optical Solitons*, Burlington: Academic Press, 2003.

[3] Y.-D. Wu, "New all-optical switch based on the spatial soliton repulsion," Opt. Express Vol. 14, No. 9, pp. 4005-4012, 2006.

[4] Y.-D. Wu, "All-optical 1 × N switching device by use of the phase modulation of spatial solitons," Appl. Opt. Vol. 44, No. 19, pp. 4144-4147, 2005.

[5] Y.-D. Wu, "New all-optical wavelength auto-router based on spatial solitons," Opt. Express Vol. 12, No. 18, pp. 4172-4177, 2004.

[6] A. Kumar and A.K. Sarma, "Soliton switching in a Kerr coupler with coupling constant dispersion: a variational analysis," Opt. Commun. Vol. 234, No. 1–6, pp. 427-432, 2004.

[7] S. Yaocheng, D. Daoxin, and H. Sailing, "Proposal for an Ultracompact Polarization-Beam Splitter Based on a Photonic-Crystal-Assisted Multimode Interference Coupler," IEEE Photon. Technol. Lett. Vol. 19, No. 11, pp. 825-827, 2007.

[8] R.A. Vicencio, M.I. Molina, and Y.S. Kivshar, "Controlled switching of discrete solitons in waveguide arrays," Opt. Lett. Vol. 28, No. 20, pp. 1942-1944, 2003.

[9] A.K. Sarma, "Vector soliton switching in a fiber nonlinear directional coupler," Opt. Commun. Vol. 284, No. 1, pp. 186-190, 2011.

[10] Q. Li, A. Zhang, and X. Hua, "Numerical simulation of solitons switching and propagating in asymmetric directional couplers," Opt. Commun. Vol. 285, No. 2, pp. 118-123, 2012.

[11] A. Ghadi and S. Mirzanejhad, "All-optical logic gates using semiconductor-based three-coupled waveguides nonlinear directional coupler," Opt. Commun. Vol. 284, No. 1, pp. 232-235, 2011.

[12] C.-D. Truong and T.-T. Le, "Power splitting ratio couplers based on MMI structures with high bandwidth and large tolerance using silicon waveguides," Photon. Nanostructures-Fundament. Appl. Vol. 11, No. 3, pp. 217-225, 2013.

[13] D. J.Y. Feng and T.S. Lay, "Compact multimode interference couplers with arbitrary power splitting ratio," Opt. Express, Vol. 16, No. 10, pp. 7175-7180, 2008.

[14] D. A. May-Arrioja, P. LiKamWa, C. Velasquez-Ordonez, and J. J. Sanchez-Mondragon "Tunable multimode interference coupler," Electron. Lett. Vol. 43, No. 13, pp. 714-716, 2007.

[15] D.A. May-Arrioja, P. LiKamWa, J.J. Sánchez-Mondragón, R.J. Selvas-Aguilar, and I. Torres-Gomez, "A reconfigurable multimode interference splitter for sensing applications," Measur. Sci. Technol. Vol. 18, No. 10, pp. 3241, 2007.

[16] J. Leuthold and C.H. Joyner, "Multimode Interference Couplers with Tunable Power Splitting Ratios," IEEE J. Lightw. Technol. Vol. 19, No. 5, pp. 700-707, 2001.

[17] O. Lahav, H. Gurgov, P. Sidorenko, O. Peleg, L. Levi, A. Fleischer, and O. Cohen, "Self-phase modulation spectral broadening in two-dimensional spatial solitons: toward three-dimensional spatiotemporal pulse-train solitons," Opt. Lett. Vol. 37, No. 24, pp. 5196-5198, 2012.

[18] O. Katz, Y. Lahini, and Y. Silberberg, "Multiple breakup of high-order spatial solitons," Opt. Lett. Vol. 33, No. 23, pp. 2830-2832, 2008.

[19] V.V. Afanasjev, J.S. Aitchison, and Y.S. Kivshar, "Splitting of high-order spatial solitons under the action of two-photon absorption," Opt. Commun. Vol. 116, No. 4–6, pp. 331-338, 1995.

[20] Y. Silberberg, "Solitons and two-photon absorption," Opt. Lett. Vol. 15, No. 18, pp. 1005-1007, 1990.

[21] J.S. Aitchison, A.M. Weiner, Y. Silberberg, M.K. Oliver, J.L. Jackel, D.E. Leaird, E.M. Vogel, and P.W.E. Smith, "Observation of spatial optical solitons in a nonlinear glass waveguide," Opt. Lett. Vol. 15, No. 9, pp. 471-473, 1990.

[22] R.A. Sammut, C. Pask, and Q.Y. Li, "Theoretical study of spatial solitons in planar waveguides," J. Opt. Soc. Am. B, Vol. 10, No. 3, pp. 485-491, 1993.

[23] J.S. Aitchison, Y. Silberberg, A.M. Weiner, D.E. Leaird, M.K. Oliver, J.L. Jackel, E.M. Vogel, and P.W.E. Smith "Spatial optical solitons in planar glass waveguides," J. Opt. Soc. Am. B, Vol. 8, No. 6, pp. 1290-1297, 1991.

[24] T. Fujisawa and M. Koshiba, "Full-Vector Finite-Element Beam Propagation Method for

Three-Dimensional Nonlinear Optical Waveguides," IEEE J. Lightw. Technol. Vol. 20, No. 10, pp. 1876-1884, 2002.

[25] A. Taflove and S.C. Hagness, *Computational Electrodynamics*, 1995.

[26] T. Yasui, M. Koshiba, and Y. Tsuji, "A Wide-Angle Finite Element Beam Propagation Method with Perfectly Matched Layers for Nonlinear Optical Waveguides," IEEE J. Lightw. Technol. Vol. 17, No. 10, pp. 1909-1915, 1999.

[27] R. Boyd, *Nonlinear Optics*, Academic Press, San Diego, 3rd Ed., 2008.

[28] K. Kawano and T. Kitoh, *Introduction to Optical Waveguide Analysis.* John Wiley & Sons, Inc., 2001.

[29] G. Sun and C.W. Trueman, "Unconditionally-stable FDTD method based on Crank-Nicolson scheme for solving three-dimensional Maxwell equations," Electron. Lett.Vol. 40, No. 10, pp. 589-590, 2004.

[30] Y. Chung and N. Dagli, "An assessment of finite difference beam propagation method," IEEE J. Quantum Electron. Vol. 26, No. 8, pp. 1335-1339, 1990.

[31] G.R. Hadley, "Transparent boundary condition for beam propagation," Opt. Lett. Vol. 16, No. 9, pp. 624-626, 1991.

Amin Ghadi was borne 1978 in Iran, and he obtained his Ph.D in 2012 from the University of Mazandaran, Iran. He subsequently has joined atomic and molecular physics department of university of Mazandaran since 2013, currently as an Assistant Professor.

His research interests are nonlinear optical effects on photonic devices, all optical switches, directional couplers and ring resonators.

Saeed Mirzanejhad was born in 1968 in Iran, and received his PhD in Amir-Kabir University of technology in Tehran in free electron laser. He joined to atomic and molecular physics department of university of Mazandaran.

His research interests are photonic devices, nonlinear optics, laser interaction with materials.

THIS PAGE IS INTENTIONALLY LEFT BLANK.

SCOPE

Original contributions relating to advances, or state-of-the-art capabilities in the theory, design, applications, fabrication, performance, and characterization of: Lasers and optical devices; Laser Spectroscopy; Lightwave communication systems and subsystems; Nanophotonics; Nonlinear Optics; Optical Based Measurements; Optical Fiber and waveguide technologies; Optical Imaging; Optical Materials; Optical Signal Processing; Photonic crystals; and Quantum optics, and any other related topics are welcomed.

INFORMATION FOR AUTHORS

International Journal of Optics and Photonics (IJOP) is an **open access** Journal, published online semiannually with the purpose of publication of original and significant contributions relating to photonic-lightwave components and applications, laser physics and systems, and laser-electro-optic technology. Please submit your manuscripts through the Web Site of the Journal (**http://www.ijop.ir**). Authors should include full mailing address, telephone and fax numbers, as well as e-mail address. Submission of a manuscript amounts to assurance that it has not been copyrighted, published, accepted for publication elsewhere, and that it will not be submitted elsewhere while under consideration.

MANUSCRIPTS

The electronic file of the manuscript including all illustrations must be submitted. The manuscript must be in double column with the format of **IJOP Paper Template** which for ease of application all over the world is in MS-Word 2003. The manuscript must include an abstract. The abstract should cover four points: statement of problem, assumptions, and methods of solutions, results and conclusion or discussion of the importance of the results. All pages, including figures, should be numbered in a single series. The styles for references, abbreviations, etc. should follow the IJOP format. For information on preparing a manuscript, please refer to the IJOP webpage at: **http://www.ijop.ir**.

Prospective authors are urged to read this instruction and follow its recommendations on the organization of their paper. References require a complete title, a complete author list, and first and last pages cited for each entry. All references should be archived material such as journal articles, books, and conference proceedings. Due to the changes of contents and accessibility over time, Web pages must be referenced as low as possible.

Figure captions should be sufficiently clear so that the figures can be understood without referring to the accompanying text. Lettering and details of the **figures** and **tables** should be large enough to be readily legible when the drawing is reduced to one-column width of the double column article. **Axes of graphs** should have self-explanatory labels, not just symbols (e.g., Electric Field rather than E). **Photographs** and **figures** must be glossy prints in electronic files with GIF or JPEG Formats.

Article Keywords are mandatory and must be included with all manuscripts. Please choose approximately 4 to 8 keywords which describe the major points or topics covered in your article.

COPYRIGHT TRANSFER FORM

Authors are required to sign an IJOP copyright transfer form before publication. *Authors must submit the signed copyright form with their manuscript.* The form is available online at **http://www.ijop.ir.**

ISSN: 1735-8590

http://www.ijop.ir